

VERY COMPACT FULL DIFFERENTIAL BANDPASS FILTER WITH TRANSFORMER INTEGRATED USING INTEGRATED PASSIVE DEVICE TECHNOLOGY

S.-M. Wu and C.-T. Kuo

Department of Electrical Engineering
National University of Kaohsiung
No. 700, Kaohsiung University Road, Nan-Tzu District,
Kaohsiung 811, Taiwan

C.-H. Chen

Department of Electrical Engineering
National Sun Yat Sen University
No. 70, Lien-Hai Road, Kaohsiung 804, Taiwan

Abstract—In this study, a very compact, second-order, full differential bandpass filter is presented. To achieve compact circuit area and system-in-package (SiP) applications, the transformer structure is integrated using integrated passive device (IPD) technology on a glass substrate. The coupled resonator synthesis method is used to achieve the bandpass filter design and suitably adjust the tapped feed-lines to obtain good impedance match at all ports. The area ($1.27\text{ mm} \times 1.27\text{ mm}$) of the bandpass filter is effectively reduced, and the performance, as measured by insertion loss (2.5 dB) and CMRR ($> 30\text{ dB}$), is still acceptable with such a compact area. Most importantly, this full differential bandpass filter is also suitable for SiP applications, as other studies implemented using glass IPD technology have demonstrated.

1. INTRODUCTION

The recent trend in electronic products development is to simultaneously achieve light weight, thinness, high performance, high density integration and low cost. Passive components play an important role

Received 17 December 2010, Accepted 19 January 2011, Scheduled 3 February 2011

Corresponding author: Sung-Mao Wu (sungmao@nuk.edu.tw).

in the design and integration of the required systems. In the past, discrete components were the norm for passive component such as those in surface-mount device technology. However, discrete components take up too much space and increase cost. A better method is to implement a print circuit board (PCB) or other substrates, such as FR4, RT/duroid 6010LM Al_2O_3 ceramic substrate [1] and low-temperature co-fired ceramic (LTCC) technology. Although this method improves performance and shortens time intervals, limiting factors still include area reduction, design flexibility for highdensity integration and cost. System on chip (SoC) is a proposed solution using many circuits integrated in a chip with CMOS processing to reduce the circuit area and achieve high density integration. But the quality factor (Q) of passive components remains a bottleneck for improvement.

The bandpass filter is an important component for the radio frequency (RF)/microwave front-end systems, used to reject noise that would interfere with signal transmission in a system. Most research on bandpass filter design uses PCBs. In [2], a conventional microstrip filter was based primarily on transmission-line structures but occupied a large area due to quarter- or half-wavelength resonator requirements. Some studies propose better solutions for reducing circuit size, such as a stepped impedance resonator (SIR) [3–5], defected ground structure (DGS) resonator [6–8], patch-via-spiral resonator [9], or net-type resonator [10]. Unfortunately, these methods are still limited in design flexibility, quality factor, and cost. Differential circuits have become increasingly important recently because of their noise rejection ability. Balanced bandpass filters (singleend input and differential output) and full differential bandpass filters (differential input and differential output) have become popular research topics. Most of these studies have used a microstrip line [11–13]. In [14], researchers used coupled-line sections and quarter-wavelength ($\lambda/4$) resonators to design a full differential bandpass filter but its area still needs further reduction. A stepped-impedance resonator (SIR) is another proposed method for full differential bandpass filter design [15]. A coupled-resonator and half-wavelength ($\lambda/2$) resonator were used in [16, 17], while a double-sided parallel-strip line (DSPSL) dual-mode resonator was proposed in [18]. However, area reduction in these studies was still limited. Integrated passive device (IPD) technology on a glass substrate is an attractive solution to the foregoing problems. IPD features lower loss than silicon substrate, high Q inductor, and good design flexibility for integration [19–22]. In IPD technology, many different substrates were adopted for circuit design, such as silicon and glass. Passive devices were almost integrated in silicon process based on SoC technology. Usually, inductors with lower quality factor were made on silicon

substrate using thin-film-metallization process. The substrate loss on silicon and thin film metallization decided the quality factor of inductors. So, glass IPD substrates used in this study are characterized by [21]:

1) using thicker Cu metal for transformer design to reduce resistive loss; 2) using CVD-deposited SiN_x as the dielectric layer of MIM capacitors; and 3) because the substrate (dielectric) loss of glass substrate is smaller than that of silicon substrate, it can be used to improve the quality factor.

It is also worth mentioning that IPD technology can easily be integrated with system-in-package (SiP) applications, prompting extensive research on transformer-based structures in IPD technology, such as impedance transformation, balanced-to-unbalanced conversion (balun), power combining and coupling circuits [23, 24]. A very compact transformer-coupled balun-integrated bandpass filter using IPD technology on glass substrate was presented in [25] reducing the bandpass filter area, providing coupling to the balanced output ports, and creating extra transmission zeros to enhance the desired stopband rejection. A cross-section of this glass IPD technology is presented in Fig. 1. The circuit design is comprised of three metal layers: metal 3 is thick copper for inductors design realizing the high Q transformers while metals 2 and 1 are thin copper (Cu) and gold (Au), respectively. A high- k (high dielectric constant) dielectric (SiN_x) layer between metals 1 and 2 allows metal-insulator-metal (MIM) capacitors to be part of the circuit design. A benzocyclobutene (BCB) layer provides cover and isolation.

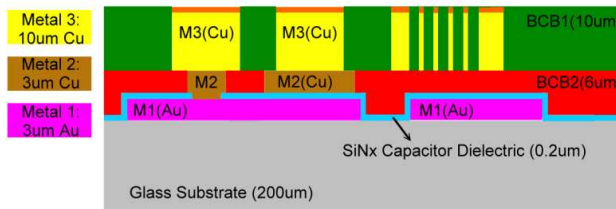


Figure 1. Cross-section of a glass IPD technology process.

This study presents a full differential bandpass filter extended from [25] using glass IPD technology for wireless local area network (WLAN) IEEE 802.11 b/g (2.4 GHz) applications. Using a planar transformer with series capacitors to provide a magnetic-dominant coupling of the coil-type resonators results in a very compact bandpass filters and increases design flexibility. Using the proposed

architecture a bandpass filter (single-end in and single-end out), a balanced bandpass filter (single-end in, and differential out), and a full differential bandpass filter (differential in and differential out) could be designed at the same time. Comparison of simulated and measured results shows that the passband frequency shifts to a high frequency because the supplied dielectric coefficient (ϵ_r) is not equal to the effective dielectric constant (ϵ_{eff}), which will be discussed in the last section of this paper. Unlike other research that has implemented PCBs or different substrates, using the glass IPD technology can effectively improve the circuit area without affecting circuit performance. The most important outcome is that a full differential bandpass filter using glass IPD technology is easily integrated with SiP applications [26–30] and enhances system design flexibility.

2. COUPLED RESONATOR ANALYSIS

The structure and equivalent circuit of a coupled resonator is shown in Fig. 2. This structure consists of two parallel resonant circuits (Resonator A and Resonator B) magnetically coupled with a transformer mutual inductance M . Each resonant circuit includes a coil inductance ($L_1 - L_2 - L_1$) resonated with a pair of dual capacitors of capacitance C achieved using a MIM capacitor. A mutual capacitance C_c is used between the two resonant circuits, representing

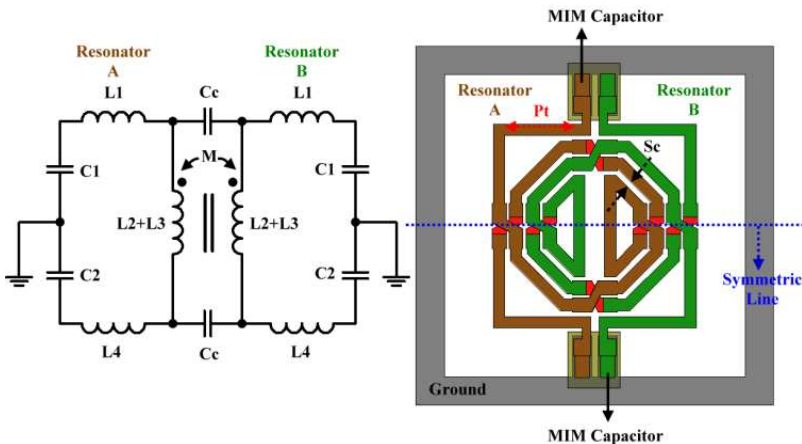


Figure 2. Equivalent circuit and physical layout of the coupled resonator in this study.

the parasitic electrical coupling between the two coil-type resonators. The symmetric line of the structure in this study is evident in Fig. 2, where the outside ring is the ground for the resonant circuit. The planar transformer is designed in an octagonal shape with the two parallel coils symmetrically interwoven side by side on metal 3. The red parallelogram shapes indicate coil underpasses, implemented on metal 1. A pair of dual capacitors located at the top and bottom of Fig. 2 uses metals 2 and 1. In this study, we applied magnetic coupling using the coupled resonator synthesis method [31]. Our method of analyzing the equivalent circuit will be explained in the following section. Because this study is an extension of [25], we focus on the full differential design and leave aside the design flow of the bandpass filter and balanced bandpass filter within this architecture.

2.1. Single Resonator

In filter design, two important parameters for applying the above-mentioned method are the coupling coefficient (k) between two resonators and the external quality factor (Q_e). Before describing the extraction of these two parameters, we will first analyze the architecture of a single resonator. Fig. 3(a) shows the structure and equivalent circuit of a single resonator. By changing the tapped feed position (Pt), the ratio between L_1 and L_2 can be determined. For a single resonator design, the resonant frequency is calculated by

$$f_s = \frac{1}{2\pi\sqrt{(L_1 + L_2)C}} \tag{1}$$

where f_s is the resonant frequency. Fig. 4 shows the input impedance of a single resonator and a double resonator; using Equation (1), the

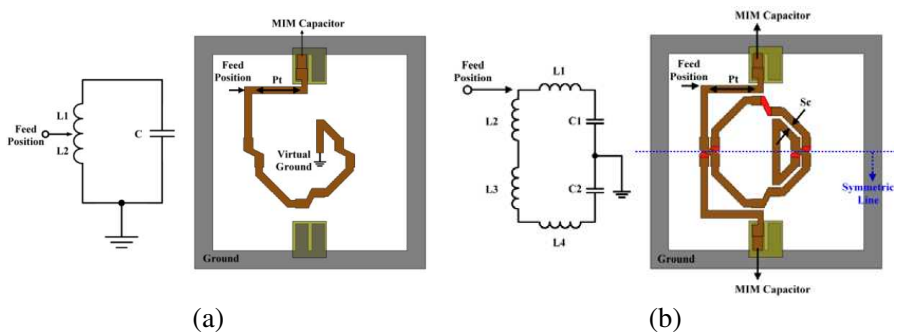


Figure 3. Equivalent circuits and physical layout of (a) single resonator and (b) double resonator.

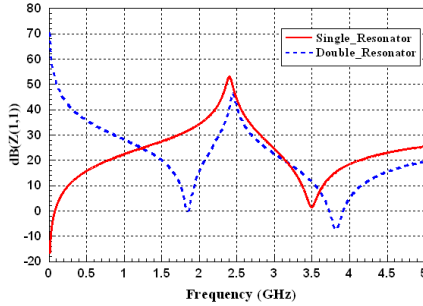


Figure 4. Input impedance of single and double resonators.

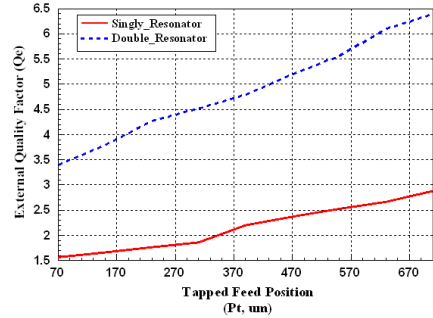


Figure 5. Calculated external quality factors of resonators versus tapped feed position.

resonant frequency can be calculated. In addition, the position of the transmission zero, which is located between 3 GHz and 4 GHz, relates to L_1 and C .

The Q_e of a single resonator can be evaluated as a function of the tapped feed position. It is often measured in terms of the normalized input admittance (y_{in}) and the group delay (τ_T) with respect to the reflection coefficient at the resonant angular frequency ω [31]. That is,

$$Q_e = \frac{\omega_0 \tau_T(\omega_0)}{4} [1 - y_{in}^2(\omega_0)] \quad (2)$$

where y_{in} can be obtained from the reflection coefficient, and τ_T can be found in its phase with respect to angular frequency. Fig. 5 shows the relationship between the tapped feed position and Q_e , which expresses whether or not there is impedance matching between the bandpass filter and the external circuit.

2.2. Double Resonator

To reduce the level of common-mode noise while achieving the desired passband response in differential-mode operation, a symmetric structure is adopted. The structure and equivalent circuit of a double resonator are shown in Fig. 3(b). It consists of inductance ($L_1 - L_2 - L_3 - L_4$) resonated with a pair of dual capacitors of capacitance C . For the purpose of the symmetric structure, we let $L_1 = L_4$, $L_2 = L_3$, and $C_1 = C_2$. The input impedance of the double resonator is presented in Fig. 4, and its resonant frequency is also determined using Equation (1). Two transmission zeros are located at 1.9 GHz and 3.9 GHz, respectively. The transmission zero at the higher

frequency is dominated by input inductance and capacitance (L_1 and C_1), while the other transmission zero is determined by L_2 , L_3 , L_4 , and C_2 . The extraction method for Q_e is the same as for single resonator. Using Equation (2), the tapped feed position versus Q_e is given in Fig. 5. It is clear that the Q_e of the double resonator approximately doubles that of the single resonator.

2.3. Extraction k

The other important parameter in a coupled-resonator filter design is the coupling coefficient (k) between the two resonators. The intensity of coupling, which dominates the bandwidth of the bandpass filter, depends on the spacing between the intertwined turns of the coils in the transformer (Sc, shows in Fig. 3(b)). According to [31], the coupling coefficient relating the two dominant resonant frequencies f_1 and f_2 can be calculated as follows:

$$k = \pm \frac{f_2^2 - f_1^2}{f_2^2 + f_1^2} \quad (3)$$

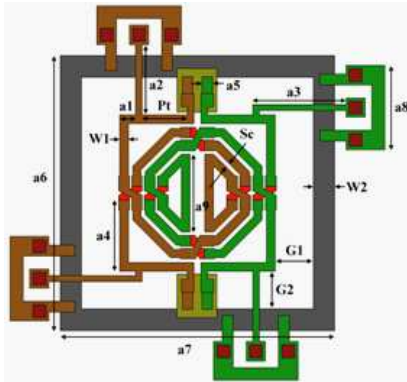
Variation in the coupling coefficient depends on the spacing and expresses how the spacing of coil inductance affects the coupling intensity.

3. FULL DIFFERENTIAL BANDPASS FILTER USING COUPLED RESONATOR

3.1. Filter Structure

The proposed full differential bandpass filter shown in Fig. 6 is composed of two symmetric resonators, based on the work in [25]. To create the symmetric structure, the proposed filter was integrated using a planar transformer with series capacitors. The target of reducing the circuit area and the level of common-mode noise while achieving the desired passband response in differential-mode operation was thereby realized.

The proposed full differential bandpass filter in Fig. 7 was implemented using an integrated transformer fabricated on glass IPD technology (glass substrate thickness = 200 μm , dielectric constant (SiNx) = 7.2, loss tangent = 0.0065, dielectric constant (BCB) = 2.7), as shown in Fig. 1. In the process of designing this bandpass filter, a full wave simulation Ansoft HFSSTM was used. For the convenience of 4-port measurement, a tapped feed trace was adjusted in four directions (east, west, south, and north). An Agilent ENA network analyzer and a Cascade probe (ACP-40-GSG, pitch 150 μm) were used



	Length(mm)		Length(mm)
W1	0.04	a2	0.326
W2	0.1	a3	0.43
G1	0.175	a4	0.33
G2	0.175	a5	0.05
Pt	0.21	a6 = a7	1.27
Sc	0.03	a8	0.39
a1	0.075	a9	0.36

Figure 6. Physical layout of the proposed full differential bandpass filter.

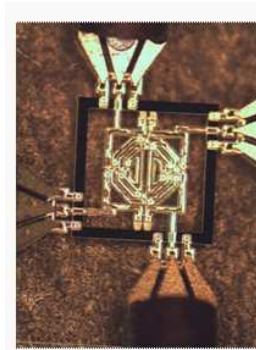


Figure 7. Photograph of the fabricated full differential bandpass filter.

to measure filter response. The 4-port S -parameters for simulation and measurement were deduced using mixed-mode S -parameters, as per [32].

3.2. Design Procedure

A second-order 0.1 dB equal-ripple Chebyshev response bandpass filter was designed with a center frequency of 2.45 GHz and a fractional bandwidth Δ of 15%. The unload quality factor (Q_u) of a coil-type resonator is 22, and the corresponding element values of the prototype are $g = 1$, $g_1 = 0.843$, $g_2 = 0.622$, and $g_3 = 1.355$. To determine the turn spacing of the coil and the tapped feed position of the full differential bandpass filter, the coupling coefficients at differential-

mode operation (k_{12}^{dd}) and the external quality factors (Q_e^{dd}) of the second-order filter prototype elements need to be calculated from [31]. These relations are given as:

$$k_{12}^{dd} = \frac{\Delta}{\sqrt{g_1 g_2}} = 0.21 \tag{4}$$

$$Q_e^{dd} = \frac{g_0 g_1}{\Delta} = \frac{g_2 g_3}{\Delta} = 5.6 \tag{5}$$

where Δ is the fractional bandwidth, and g_i is the i th prototype element value. In addition, for a second-order equal-ripple Chebyshev bandpass filter design, the insertion loss at the passband can be estimated by the formula given in [31], reproduced below:

$$IL_{\omega_0}(\text{dB}) \approx \frac{4.343}{\Delta \cdot Q_u} (g_1 + g_2) = 1.92 \tag{6}$$

According to the above-described design procedure, the full differential bandpass filter corresponds with the design specifications.

3.3. Differential Mode Response

Figures 8(a) and 8(b) show comparisons between measured and simulated differential-mode responses of the proposed full differential bandpass filter in Fig. 6. The measured passband frequency is 2.9 GHz. The minimum insertion loss (S_{21}^{dd}) and return loss (S_{11}^{dd}) are 3.47 dB and 7.2 dB, respectively. The fabricated full differential bandpass filter has a size of 1.27 mm \times 1.27 mm, and the transmission zero is created at 4 GHz.

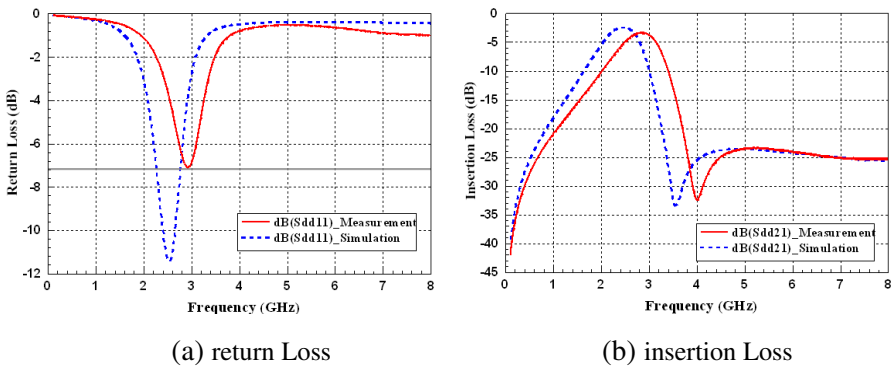


Figure 8. Measured and simulated differential-mode responses for the proposed full differential bandpass filter.

From the comparison, it is evident that the measurement passband frequency shifts from 2.45 GHz to 2.9 GHz, and the transmission zero shifts from 3.57 GHz to 4 GHz. The reason for this frequency shift is that the supplied dielectric coefficient (ϵ_r) from IC foundry services is not the effective dielectric constant (ϵ_{eff}) within the circuit design. However, appropriately adjusting the dielectric coefficient of the simulated parameter improves the results.

3.4. Common Mode Response

Figure 9(a) presents a comparison between measured and simulated common-mode responses of the proposed full differential bandpass filter in Fig. 6. The measured common-mode response is suppressed below -25 dB up to 8 GHz. As suggested by [33], the common-mode rejection ratio (CMRR) defined by

$$\text{CMRR} = 20 \cdot \log \frac{|s_{21}^{dd}|}{|s_{21}^{cc}|} \quad (\text{dB}) \quad (7)$$

was adopted as the performance measure for the level of common-mode suppression around the full differential bandpass filter. The CMRR of the proposed bandpass filter is presented in Fig. 9(b). The maximum CMRR is 28.4 dB at 2.9 GHz, with all the CMRR values above 25 dB ranging from 2.45 GHz to 3.29 GHz.

In Table 1, the full differential bandpass filter realized in this study is summarized and compared with other studies. Note that the dimension of the present bandpass filter is much smaller than in other studies. Although the performance is not excellent, the full differential

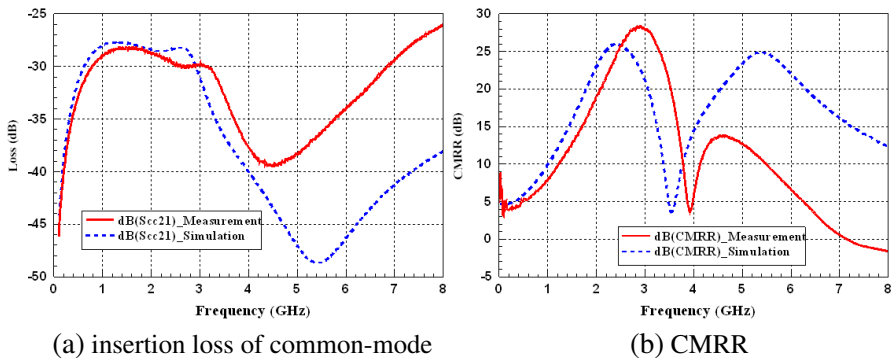


Figure 9. Measured and simulated comparison of common-mode response for proposed full differential bandpass filter.

Table 1. Comparison of measured specifications and size between this work and several recent references.

Reference	Technology	Frequency	Chip Dimension (mm ²)	S_{21}^{dd} (dB)	CMRR in passband (dB)
This work	Glass IPD	2.45 GHz	1.27×1.27	3.47	> 25
This work after adjusting tapped feed position	Glass IPD	2.45 GHz	1.27×1.27	1.5	> 30
[14]	FR4 substrate	2 GHz	35.9×10.9	2.3	> 22.5
[15]	FR4 substrate	1.02 GHz	33.4×36.2	3.51	N.A.
[16]	FR4 substrate	1.025 GHz	38.4×56	3.8	> 45
[17]	Taconic RF-60A-0310 substrate	1.57 GHz	26.7×23.1	1.95	> 22

bandpass filter design using glass IPD technology is still acceptable for SiP applications. The most important fact is that the filter design fabricated on glass IPD technology is easily integrated with the CMOS process, achieving the target of being usable in SiP applications.

4. DISCUSSION

The proposed full differential bandpass filter still has some flaws to be addressed. As indicated in the previous section, the shift in measurement passband frequency and the mismatch caused by different tapped feed position need to be adjusted. A discussion of these flaws follows.

4.1. Frequency Shifting

From the measurement results, it is clear that the passband frequency shifts to a high frequency. The speculated reason is that the supplied dielectric coefficient (ϵ_r) is not equal to the effective dielectric constant (ϵ_{eff}). To verify this inference, the ϵ_r of the high-k dielectric was adjusted from 7.2 to 5.39. The inferential result was realized using Ansoft HFSSTM simulator.

Figures 10(a) and (b) and Fig. 11(a) show differential-mode response and common-mode response, respectively, comparing measured and simulated modified dielectric constants. Fig. 11(b) compares CMRR results. That the curves in these comparative results

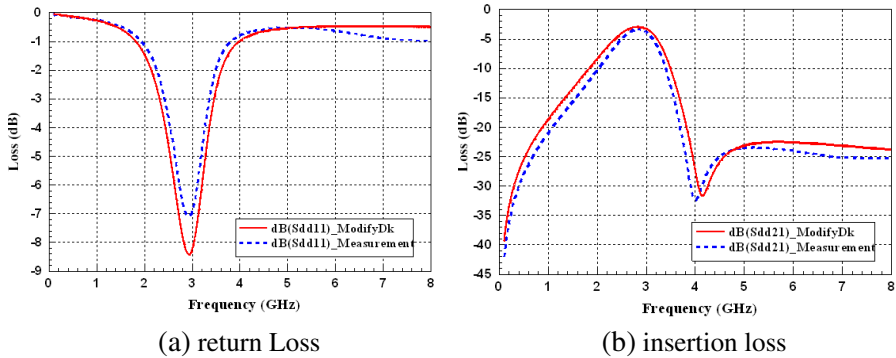


Figure 10. Modified ϵ_r and measured comparison of differential-mode response for proposed full differential bandpass filter.

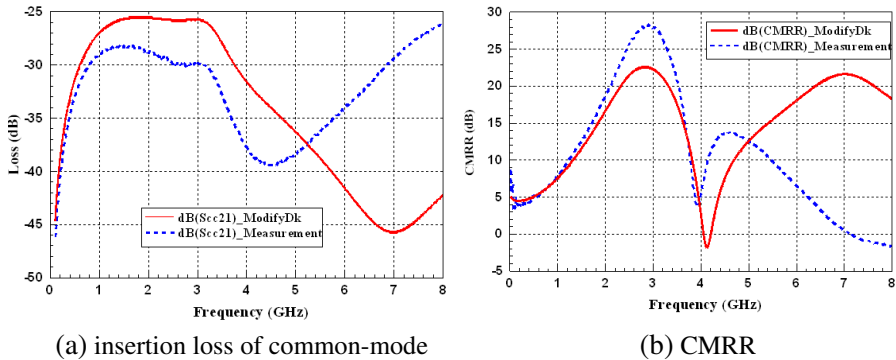


Figure 11. Modified ϵ_r and measured comparison of common-mode response for proposed full differential bandpass filter.

almost overlap could be proof that the passband frequency shift is caused by the effective dielectric constant.

4.2. Tapped Feed Position

From the above comparison between simulated and measured results, it is evident that the tapped feed position is incorrect, resulting in the response not corresponding with the design specification. In other words, the return loss of the differential-mode response for the second-order 0.1 dB equal-ripple Chebyshev response design should have exhibited two reflection zeros. For this reason, the tapped feed position needed to be adjusted again. In addition, to conveniently conduct 4-port measurement with a Cascade probe (ACP-40-GSG, pitch 150 μm),

the measurement traces were turned in four directions (east, west, south, and north), as shown in Fig. 7. To improve the CMRR of the proposed bandpass filter and simultaneously adjust the tapped feed position, direct differential measurement with the cascade probe (ACP-40-GSGSG, pitch 150 μm) was adopted (Fig. 12). Fabrication of the adjusted full differential bandpass filter is now being carried out by the National Chip Implementation Center (CIC), Taiwan, which provides the IC foundry services. Follow-up measurements will be presented after fabrication is complete. Figs. 13 and 14 show the differential-mode and common-mode responses, respectively. The minimum insertion loss (S_{21}^{dd}) is 1.5 dB, and the return loss (S_{11}^{dd}) is 11.9 dB. Up to 8 GHz the common-mode response is suppressed below 30 dB. The CMRR in particular, shown in Fig. 15, improves up to and beyond 30 dB.

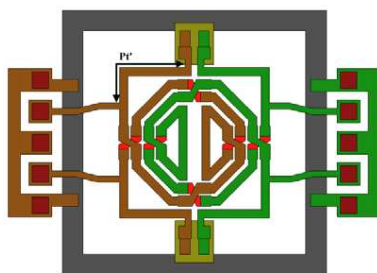


Figure 12. Adjusted tapped feed position for the physical layout of the proposed full differential bandpass filter ($Pt' = 0.485\text{ mm}$).

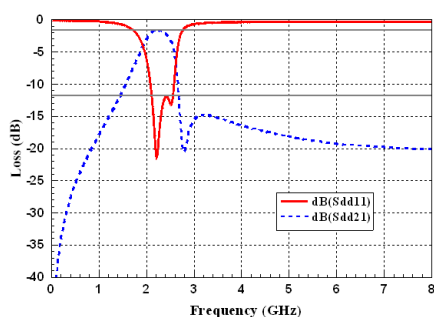


Figure 13. Adjusted tapped feed position differential-mode response for proposed full differential bandpass filter.

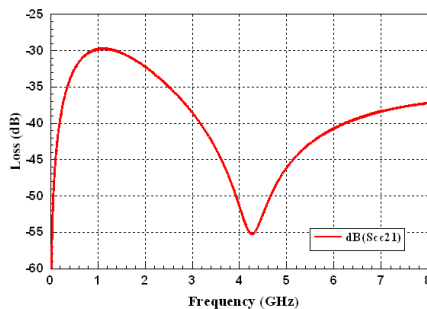


Figure 14. Adjusted tapped feed position common-mode response for proposed full differential bandpass filter.

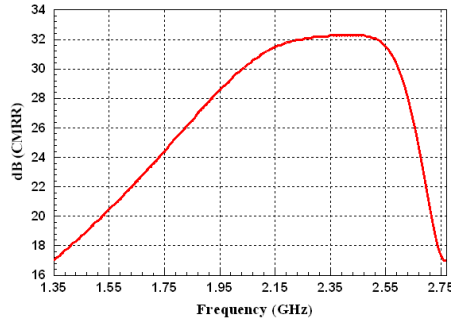


Figure 15. Adjusted tapped feed position CMRR for proposed full differential bandpass filter.

5. CONCLUSION

In this study, a very compact full differential bandpass filter using glass IPD technology has been presented. The filter effectively reduced circuit area improved the quality factor of passive components and was easily integrated for SiP applications. Although process variation and an incorrect tapped feed position affected circuit performance, high density integration and application were achievable after slight adjustments. Generally, the proposed full differential bandpass filter exhibits the following attractive features. First, its area ($1.27 \text{ mm} \times 1.27 \text{ mm}$) is much smaller than others in the literature. Second, the center frequency in this study (2.45 GHz) is commonly bands for wireless communication bands. Third, performance, as gauged by insertion loss (2.5 dB) and CMRR ($> 30 \text{ dB}$), is still acceptable for such a compact area. Last, the proposed bandpass filter, as others implemented on glass IPD technology, is proven to be suitable for SiP applications. This proposed full differential bandpass filter will be easily integrated to enhance system design flexibility.

REFERENCES

1. Kung, C.-Y., Y.-C. Chen, S.-M. Wu, C.-F. Yang, and J.-S. Sun, "A novel compact 2.4/5.2 GHz dual wideband bandpass filter with deep transmission zero," *Journal of Electromagnetic Waves and Applications*, Vol. 25, No. 5–6, 617–628, 2011.
2. Razalli, M. S., A. Ismail, M. A. Mahdi, and M. N. Bin Hamidon, "Novel compact microstrip ultra-wideband filter utilizing short-

- circuited stubs with less vias,” *Progress In Electromagnetics Research*, Vol. 88, 91–104, 2008.
3. Yang, R.-Y., C.-M. Hung, C.-Y. Hung, and C.-C. Lin, “Design of a high band isolation diplexer for GPS and WLAN system using modified stepped-impedance resonators,” *Progress In Electromagnetics Research*, Vol. 107, 101–114, 2010.
 4. Yang, R.-Y., C.-M. Hung, C.-Y. Hung, and C.-C. Lin, “A high performance bandpass filter with a wide and deep stopband by using square stepped impedance resonators,” *Journal of Electromagnetic Waves and Applications*, Vol. 24, No. 11–12, 1673–1683, 2010.
 5. Wu, H.-W. and R.-Y. Yang, “Design of a triple-passband microstrip bandpass filter with compact size,” *Journal of Electromagnetic Waves and Applications*, Vol. 24, No. 17–18, 2333–2341, 2010.
 6. Chen, J., Z.-B. Weng, Y.-C. Jiao, and F.-S. Zhang, “Lowpass filter design of hilbert curve ring defected ground structure,” *Progress In Electromagnetics Research*, Vol. 70, 269–280, 2007.
 7. NaghshvarianJahromi, M., “Novel compact meta-material tunable quasi elliptic band-pass filter using microstrip to slotline transition,” *Journal of Electromagnetic Waves and Applications*, Vol. 24, No. 17–18, 2371–2382, 2010.
 8. Shen, W., W. Y. Yi, and X.-W. Sun, “Compact microstrip tri-section bandpass filters with mixed couplings,” *Journal of Electromagnetic Waves and Applications*, Vol. 24, No. 13, 1807–1816, 2010.
 9. Lin, S. C., C. H. Wang, and C. H. Chen, “Novel patch-via-spiral resonators for the development of miniaturized bandpass filters with transmission zeros,” *IEEE Transactions on Microwave Theory and Techniques*, Vol. 55, 137–146, 2007.
 10. Chen, C. F., T. Y. Huang, and R. B. Wu, “Novel compact net-type resonators and their applications to microstrip bandpass filters,” *IEEE Transactions on Microwave Theory and Techniques*, Vol. 54, 755–762, 2006.
 11. Lim, T. B. and L. Zhu, “Differential-mode wideband bandpass filter with three transmission zeros under common-mode operation,” *Asia Pacific Microwave Conference, APMC 2009*, 159–162, 2009.
 12. Lim, T. B. and L. Zhu, “A differential-mode wideband bandpass filter on microstrip line for UWB application,” *IEEE Microwave and Wireless Components Letters*, Vol. 19, 632–634, 2009.

13. Lim, T. B. and L. Zhu, "Differential-mode ultra-wideband bandpass filter on microstrip line," *Electronics Letters*, Vol. 45, 1124–1125, 2009.
14. Wu, C. H., C. H. Wang, and C. H. Chen, "Novel Balanced coupled-line bandpass filters with common-mode noise suppression," *IEEE Transactions on Microwave Theory and Techniques*, Vol. 55, 287–295, 2007.
15. Wu, C. H., C. H. Wang, and C. H. Chen, "Stopband-extended balanced bandpass filter using coupled stepped-impedance resonators," *IEEE Microwave and Wireless Components Letters*, Vol. 17, 507–509, 2007.
16. Wu, C. H., C. H. Wang, and C. H. Chen, "Balanced coupled-resonator bandpass filters using multisection resonators for common-mode suppression and stopband extension," *IEEE Transactions on Microwave Theory and Techniques*, Vol. 55, 1756–1763, 2007.
17. Jin, S. and X. Quan, "Balanced bandpass filters using center-loaded half-wavelength resonators," *IEEE Transactions on Microwave Theory and Techniques*, Vol. 58, 970–977, 2010.
18. Shi, J., J. X. Chen, and Q. Xue, "A novel differential bandpass filter based on double-sided parallel-strip line dual-mode resonator," *Microwave and Optical Technology Letters*, Vol. 50, 1733–1735, 2008.
19. Zoschke, K., M. J. Wolf, M. Topper, O. Ehrmann, T. Fritsch, K. Kaletta, F. J. Schmuckle, and H. Reichl, "Fabrication of application specific integrated passive devices using wafer level packaging technologies," *IEEE Transactions on Advanced Packaging*, Vol. 30, 359–368, 2007.
20. Clearfield, H. M., J. L. Young, S. D. Wijeyesekera, and E. A. Logan, "Wafer-level chip scale packaging: Benefits for integrated passive devices," *IEEE Transactions on Advanced Packaging*, Vol. 23, 247–251, 2000.
21. Wang, C.-C., H.-A. Yang, Y. C. Shyu, M.-H. Li, C.-T. Chiu, and C.-P. Hung, "Analysis of high performance RF integrated passive circuits using the glass substrate," *IEEE 9th VLSI Packaging Workshop of Japan, VPWJ 2008*, 135–138, 2008.
22. Ulrich, R. and L. Schaper, *Integrated Passive Component Technology*, 1st Edition, Wiley-IEEE Press, 2003.
23. Long, J. R., "Monolithic transformers for silicon RF IC design," *IEEE Journal of Solid-state Circuits*, Vol. 35, 1368–1382, 2000.
24. Huang, C. H., T.-C. Wei, T.-S. Horng, J.-Y. Li, C.-C. Chen, C.-

- C. Wang, C.-T. Chiu, and C.-P. Hung, "Design and modeling of planar transformer-based silicon integrated passive devices for wireless applications," *IEEE Radio Frequency Integrated Circuits Symposium, RFIC 2009*, 167–170, 2009.
25. Chen, C.-H., C.-H. Huang, T.-S. Horng, S.-M. Wu, C.-T. Chiu, C.-P. Hung, J.-Y. Li, and C.-C. Chen, "Very compact transformer-coupled balun-integrated bandpass filter using integrated passive device technology on glass substrate," *2010 IEEE MTT-S International Microwave Symposium Digest (MTT)*, 1372–1375, 2010.
 26. Hongtak, L., P. Changkun, and H. Songcheol, "A Quasi-four-pair class-E CMOS RF power amplifier with an integrated passive device transformer," *IEEE Transactions on Microwave Theory and Techniques*, Vol. 57, 752–759, 2009.
 27. Chen, H.-K., Y.-C. Hsu, T.-Y. Lin, D.-C. Chang, Y.-Z. Juang, and S.-S. Lu, "CMOS wideband LNA design using integrated passive device," *IEEE MTT-S International Microwave Symposium Digest, MTT'09*, 673–676, 2009.
 28. Grima, M. L., S. Barth, S. Bosse, B. Jarry, P. Gamand, P. Meunier, and B. Barelaud, "A differential SiP (LNA-filter-mixer) in silicon technology for the SKA project," *European Microwave Conference*, 1129–1132, 2007.
 29. Zampardi, P., "Performance and modeling of Si and SiGe for power amplifiers," *2007 Topical Meeting on Silicon Monolithic Integrated Circuits in RF Systems*, 13–17, 2007.
 30. Yu, J.-I., J.-M. Yook, J.-C. Park, C.-H. Kim, and Y.-S. Kwon, "Compact front end modules for WLAN applications with integrated passive devices using selectively anodized aluminum substrate," *2010 European Microwave Integrated Circuits Conference (EuMIC)*, 329–332, 2010.
 31. Hong, J.-S. G. and M. J. Lancaster, *Microstrip Filters for RF/Microwave Applications*, Wiley, New York, 2001.
 32. Bockelman, D. E. and W. R. Eisenstadt, "Combined differential and common-mode scattering parameters: Theory and simulation," *IEEE Transactions on Microwave Theory and Techniques*, Vol. 43, 1530–1539, 1995.
 33. Eisenstadt, W. R., B. Stengel, and B. M. Thompson, *Microwave Differential Circuit Design Using Mixed-mode S-parameters*, Artech House, Boston, 2006.